J|A|C|S
ARTICLES
Published on Web 06/16/2006

Vanadium Silicalite-1 Nanoparticles Deposition onto the Mesoporous Walls of SBA-15. Mechanistic Insights from a Combined EPR and Raman Study

Mario Chiesa,[†,‡] Vera Meynen,[§] Sabine Van Doorslaer,[*,‡] Pegie Cool,[§] and Etienne F. Vansant[§]

Contribution from the Dipartimento di Chimica IFM, Università di Torino and NIS, Nanostructured Interfaces and Surfaces Centre of Excellence,via P. Giuria 7, 10125, Torino, Italy, Laboratory for Spectroscopy in Biophysics and Catalysis, Department of Physics, University of Antwerp, Universiteitsplein 1, B-2610 Wilrijk, Belgium, and Laboratory of Adsorption and Catalysis, Department of Chemistry, University of Antwerp, Universiteitsplein 1, B-2610 Wilrijk, Belgium

Received March 9, 2006; E-mail: sabine.vandoorslaer@ua.ac.be

Abstract: Continuous Wave (CW) and pulsed Electron Paramagnetic Resonance (EPR) spectroscopy in conjunction with Raman spectroscopy are used to investigate the properties of Vanadium Silicalite-1 (VS-1) nanoparticles dispersed onto the mesoporous walls of SBA-15 silica. The properties of the deposited zeolite nanoparticles are found to be remarkably different from those of the full grown VS-1 zeolite. Monitoring of the local VO^{2+} environment in the noncalcined nanoparticles in SBA-15 reveals that, in contrast to the full grown zeolite case, these sites are highly hydrophilic. Also, the stability of the TPAOH template is found to be affected by acidification of the nanoparticles. These results promise to be of great importance in elucidating the formation mechanism of TPAOH-templated zeolitic nanoparticles and their incorporation in mesoporous silica materials

1. Introduction

Microporous (ϕ < 2 nm) zeolites are well-known as good industrial catalysts and adsorbents. Due to their uniform and molecular-sized pores, they are responsible for the shape selectivity of various reactions. However, due to the limited pore sizes of the zeolites, the accessibility of bulky molecules is low. Materials with an increased pore size are thus needed for biological applications or for fine chemical synthesis, allowing free diffusional access of reactants to and egress of products from the catalyst. Unstinting efforts in this direction have produced a wide variety of mesoporous (siliceous and non-siliceous) materials whose properties have been harnessed to facilitate the catalytic turnover of quite bulky molecules.[1,2] Among these materials, SBA-15, a mesoporous hexagonal silica system with large tailorable uniform pores (3−15 nm), was found to be particularly promising.[3−5] The essential architectural features of this material consist of thick microporous pore walls (3−6 nm), which confer to the structure a high thermal and hydrothermal stability compared to other mesoporous compounds.[6] The combined micro- and mesoporosity, the improved stability, and the possibility to prepare SBA-15 from cheap silicon sources[7−10] and via fast synthesis procedures[11] have led to a great deal of interest in this material.

A lot of research has been done to activate SBA-15 with various transition metal oxides in order to obtain large pore catalysts allowing high diffusion rates and a catalytic activity for bulky molecules.[12−16] Recently, a more mechanically stable analogue of SBA-15, namely plugged hexagonal templated silica (PHTS), was developed. The material is synthesized by an increased silica/surfactant ratio during the SBA-15 synthesis, which creates microporous amorphous nanoparticles (plugs) inside of the mesoporous channels of SBA-15.[17−21] Similar to SBA-15, it is composed of hexagonally ordered mesopores with

† Università di Torino and NIS.
‡ Department of Physics, University of Antwerp.
§ Department of Chemistry, University of Antwerp.

(1) Soler-Illia, G. J.; Sanchez, C.; Lebeau, B.; Patarin, J. *Chem. Rev.* **2002**, *102*, 4093.
(2) Taguchi, A.; Schüth, F. *Microporous Mesoporous Mater.* **2005**, *77*, 1.
(3) Zhao, D.; Feng, J.; Huo, Q.; Melosh, N.; Fredrickson, G. H.; Chmelka, B. F.; Stucky, G. D. *Science* **1998**, *279*, 548.
(4) Kruk, M.; Jaroniec, M.; Ko, C. H.; Ryoo, R. *Chem. Mater.* **2000**, *12*, 1961.
(5) Bennadja, Y.; Beaunier, P.; Margolese, D.; Davidson, A. *Microporous Mesoporous Mater.* **2001**, *44*−*45*, 147.
(6) Cassiers, K.; Linssen, T.; Mathieu, M.; Benjelloun, M.; Schrijnemakers, K.; Van Der Voort, P.; Cool, P.; Vansant, E. F. *Chem. Mater.* **2002**, *14*, 2317.
(7) Kim, J. M.; Stucky, G. D. *Chem Commun.* **2000**, 1159.
(8) Kim, S. S.; Pauly, T. R.; Pinnavaia, T. J. *Chem. Commun.* **2000**, 1661.
(9) Joo, S. H.; Ryoo, R.; Kruk, M.; Jaroniec, M. *J. Phys. Chem. B* **2002**, *106*, 4640.
(10) Choi, M.; Heo, W.; Kleitz, F.; Ryoo, R. *Chem. Commun.* **2003**, 1340.
(11) Newalkar, B. L.; Komarneni, S. *Chem. Commun.* **2002**, 1774.
(12) Kustrowski, P.; Chmielarz, L.; Dziembaj, R.; Cool, P.; Vansant, E. F. *J. Phys. Chem. A* **2005**, *109*, 330.
(13) Fornés, V.; López, C.; López, H. H.; Martinez, A. *Appl. Catal., A* **2003**, *249*, 345.
(14) Chiu, J. J.; Pine, D. J.; Bishop, S. T.; Chmelka, B. F. *J. Catal.* **2004**, *221*, 400.
(15) Zhang, W.-H.; Lu, J.; Han, B.; Li, M.; Xiu, J.; Ying, P.; Li, C. *Chem. Mater.* **2002**, *14*, 3413.
(16) Miller, C. J.; O'Hare, D. *Chem. Commun.* **2004**, 1710.
(17) Van Der voort, P.; Ravikovitch, P. I.; De Jong, K. P.; Neimark, A. V.; Janssen, A. H.; Benjelloun, M.; Van Bavel, E.; Cool, P.; Weckhuysen, B. M.; Vansant, E. F. *Chem. Commun.* **2002**, 1010.

thick pore walls, perforated with micropores. In addition, PHTS contains a tunable amount of extra amorphous microporous silica nanoparticles (plugs) inside the mesopores, which generate a tailorable amount of open and narrowed (plugged) pores. The pillaring effect of the nanoparticles is responsible for the higher mechanical stability of the PHTS system compared to other existing mesoporous materials.[17,18,22] Moreover, it was found that the nanoparticles (plugs) influence the adsorption and diffusion of molecules within the mesoporous channels.[23−26] Because of these enhanced properties, PHTS is a promising candidate for adsorbents, encapsulating media, catalysis, etc. However, the amorphous nature of the plugs could limit their practical use since the adsorption capacity and selectivity is low.

Therefore, a new PHTS type material (SBA-VS-15) was developed by some of us,[27] in which vanadium-activated zeolitic nanoparticles (vanadium silicalite-1 (VS-1)) were deposited inside the mesoporous channels of SBA-15 by use of a postsynthesis dry impregnation with VS-1 zeolite nanoparticles. With this method, the plugs and the catalytically active element were simultaneously deposited inside the mesopores. Evidence that the nanoparticles are deposited in the SBA-15 nanopores comes from N_2-sorption isotherms of the pure SBA-15 and SBA-15 after impregnation with zeolitic nanoparticles of vanadiumsilicalite-1 (denoted as SBA-VS), which are shown in the Supporting Information. SBA-VS gives rise to an isotherm with the same characteristics as those of the recently developed PHTS. The nitrogen sorption isotherms at −196 °C of SBA-VS show a one-step capillary condensation, indicating the filling of the uniform mesopores. However, in contrast to the pure SBA-15, the SBA-15 containing VS-1 nanoparticles exhibits a two-step desorption. The first desorption step is similar to desorption in pure SBA-15 and is assigned to desorption of nitrogen from the open mesopores according to the normal Kelvin model. The second desorption step can be attributed to the dispersed zeolitic nanoparticles (plugs of vandiumsilicalite-1) within the mesopores, narrowing parts of the mesoporous channels and creating inkbottle-like sections within the mesopores (the narrowed mesopores).[17−20,28] By changing the amount of nanoparticles deposited, the ratio of open to narrowed pores, the vanadium content and the increase in microporosity can be controlled.[27] The basic nanoparticles solution before acidification and deposition evolves into the final full-grown vanadium silicalite-1 zeolite during a hydrothermal treatment.

Materials that combine the properties of mesoporous materials with those of selective and active microporous zeolites are the focus of a great amount of new and important research activities.[27,29−32] Different theories, formation mechanisms, and structural models of the zeolite nanoparticles have been proposed in the literature, often with diametrically opposite opinions.[33−35] Therefore, it is unclear whether these zeolite nanoparticles have the same properties as the full-grown zeolite and whether use of these nanoparticles in different processes (like in depositions, synthesis of mesoporous materials, extraction, etc.) changes their properties. In this work we show that the use of continuous wave (CW) and pulsed EPR spectroscopic techniques coupled with infrared (IR) and Raman spectroscopy provides detailed information on this problem. In particular by monitoring the local coordination environment of the VO^{2+} ions in noncalcined vanadium silicalite-1 nanoparticles deposited inside the mesoporous channels of SBA-15 materials, we find important differences in the characteristics of the noncalcined zeolite nanoparticles compared to the full-grown (noncalcined) zeolites. Comparative analyses of the vanadium silicalite nanoparticles with the full-grown vanadium silicalite-1 zeolite under different conditions were performed which allowed us to gain new insights on the questions relative to the mechanism of vanadyl incorporation and the influence of pH in the growth of VS-1 zeolites. From the results of the EPR study, it is clear that pH is an important parameter for zeolite formation. In addition, stability of the vanadyl species in the deposited nanoparticles and stability of the template of the zeolite were found to be dependent on storage of the noncalcined samples and pH.

We are convinced that these data are of great importance in order to understand and to control synthesis mechanisms in which zeolitic precursor solutions are used in different processes to form new types of mesoporous materials with zeolitic characteristics.

2. Experimental Section

2.1. Materials Synthesis. The mesoporous SBA-15 materials were synthesized using 4 g of pluronic P123 triblock copolymer ($EO_{20}PO_{70}EO_{20}$) dissolved in 150 mL of 2 M HCl aqueous solution. Subsequently, 8.5 g of TEOS (tetraethyl orthosilicate) was added to the solution and stirred vigorously at 45 °C for 7.5 h. The composition of the SBA-15 synthesis gel consists of the molar ratio 1 TEOS/5.87 HCl/194 H_2O/0.017 P123. After an aging time of 15 h at 80 °C the white precipitate was filtered, washed, and dried. Finally, the product was calcined under ambient atmosphere up to 550 °C for 6 h with a heating rate of 1 °C per min.

A vanadium silicalite-1 (VS-1) nanoparticles suspension was prepared by dissolving tetrapropylammoniumhydroxide (TPAOH) 20% solution (Aldrich) as a template in water. TEOS was added as a silica source. Subsequently, the solution TPAOH/TEOS/H_2O with molar ratio 1:6.4:100 was heated to about 70 °C. After evaporation of 50% of the solution, the clear solution was cooled to room temperature. Then, 0.3 g of $VOSO_4$ in 30 mL of water was added to about 15 mL of clear solution under vigorous stirring. Afterward, this clear solution was aged at room temperature for a duration of 5 days. The preparation of the

(18) Van Der Voort, P.; Ravickovitch, P. I.; De Jong, K. P.; Benjelloun, M.; Van Bavel, E.; Janssen, A. H.; Neimark, A. V.; Weckhuysen, B. M.; Vansant, E. F. *J. Phys. Chem. B* **2002**, *106*, 5873.
(19) Van Bavel, E.; Cool, P.; Aerts, K.; Vansant, E. F. *J. Phys. Chem. B* **2004**, *108*, 5263.
(20) Kruk, M.; Jaroniec, M.; Joo, S. H.; Ryoo, R. *J. Phys. Chem. B* **2003**, *107*, 2205.
(21) Sauer, J.; Kaskel, S.; Janicke, M.; Schüth, F. (Galarneau, A., Di Renzo, F., Fajula, F., Vedrine, J., Eds.) Zeolites and mesoporous materials at the dawn of the 21st century. *Stud. Surf. Sci. Catal.* **2001**, *135*, 315.
(22) Lee, J.; Park, Y.; Kim, P.; Kim, H.; Yi, J. *Chem. Mater.* **2004**, *14*, 1050.
(23) Janssen, A. H.; Van Der Voort, P.; Koster, A. J.; De Jong, K. P. *Chem. Commun.* **2002**, 1632.
(24) Meynen, V.; Segura, Y.; Mertens, M.; Cool, P.; Vansant, E. F. *Microporous Mesoporous Mater.* **2005**, *85* (1−2), 119.
(25) Van Bavel, E.; Meynen, V.; Cool, P.; Lebeau, K.; Vansant, E. F. *Langmuir* **2005**, *21*, *6*, 2447.
(26) Kortunov, P.; Valiullin, R.; Kärger, J.; Meynen, V.; Vansant, E. F. *Diffusion Fundamentals (online journal)* **2005**, *2*, 95.
(27) Meynen, V.; Beyers, E.; Cool, P.; Vansant, E. F.; Mertens, M.; Weyten, H.; Lebedev, O. I.; Van Tendeloo, G. *Chem. Commun.* **2004**, 898.
(28) Groen, J. C.; Peffer, L. A. A.; Pérez-Ramírez, J. *Microporous Mesoporous Mater.* **2003**, *60*, 1.
(29) Kirschhock, C. E. A.; Kremer, S. P. B.; Veramant, J.; Van Tendeloo, G.; Jacobs, P. A.; Martens, J. A. *Chem.—Eur. J.* **2005**, *11*, 4036.
(30) Zhang, Z.; Han, Y.; Zhu, L.; Wang, R.; Yu, Y.; Wiu, S.; Zhao, D.; Xiao, F.-S. *Angew. Chem., Int. Ed.* **2001**, *40* (7), 1255.
(31) Carr, C. S.; Kaskel, S.; Shantz, D. F. *Chem. Mater.* **2004**, *16*, 3139.
(32) Liu, Y.; Zhang, W.; Pinnavia, T. J. *J. Am. Chem. Soc.* **2000**, *122*, 8791.
(33) Kirschhock, C. E. A.; Ravishankar, R.; Jacobs, P. A.; Martens, J. A. *J. Phys. Chem. B.* **1999**, *103*, 11021.
(34) Cundy, C. S.; Cox, P. A. *Microporous Mesoporous Mater.* **2005**, *82* (1−2), 1.
(35) Kragten, D. D.; Fedeyko, J. M.; Sawant, K. R.; Rimer, J. D.; Vlachos, D. G.; Lobo, R. F.; Tsapatsis, M. *J. Phys. Chem. B* **2003**, *107*, 10006.

full-grown zeolite VS-1 was identical, with the exception of the aging period that was replaced by a hydrothermal treatment of 5 days at 180 °C. After dilution and acidification with 0.6 M HCl to pH 1, the clear solution of VS-1 nanoparticles was deposited by means of dry impregnation inside of the calcined SBA-15 samples. This final product (hereafter named SBA-VS) was dried in ambient atmosphere and calcined similarly to the calcination of the pure SBA-15 samples. For the EPR study, noncalcined samples were used.

2.2. Materials Characterization. CW- and Pulse-EPR spectra were recorded on a Bruker ESP 380E operating at a microwave (mw) frequency of 9.77 GHz and equipped with a liquid Helium cryostat (Oxford Inc.). CW-EPR spectra were recorded at 1 mW mw power, 100 kHz modulation frequency, and 0.3 mT modulation amplitude. The CW-EPR spectra were simulated using the EPRsim32 program.[36]

All pulse EPR experiments were taken at 4 K, with a repetition rate of 1 kHz.

Electron-Spin−Echo (ESE) Detected EPR. The experiments were carried out with the pulse sequence: $\pi/2 - \tau - \pi - \tau - echo$, with mw pulse lengths $t_{\pi/2} = 16$ ns and $t_\pi = 32$ ns and a τ value of 200 ns.

Hyperfine Sublevel Correlation (HYSCORE)[37] experiments were carried out with the pulse sequence $\pi/2 - \tau - \pi/2 - t_1 - \pi - t_2 - \pi/2 - \tau -$ echo with mw pulse length $t_{\pi/2} = 16$ ns and $t_\pi = 16$ ns. The time intervals t_1 and t_2 were varied in steps of 16 ns starting from 96 to 3288 ns. Two different τ values were chosen ($\tau = 96$ ns and 176 ns). An eight-step phase cycle was used to eliminate unwanted echoes. The time traces of the HYSCORE spectra were baseline corrected with a third-order polynomial, apodized with a Hamming window and zero filled. After two-dimensional Fourier transformation, the absolute value spectra were calculated. The spectra were added for the different τ values in order to eliminate blind-spot effects. The HYSCORE spectra were simulated using a program developed at the ETH Zurich.[38]

In situ DRIFT (Diffuse Reflectance Infrared Fourier Transform) spectra were measured on a Nicolet 20SXB FTIR spectrometer equipped with an in situ DRIFT cell (Spectra-Tech) and an MCT detector. The samples were mixed with KBr (98% KBr, 2% sample). Resolution was set to 4 cm^{-1}, and 500 scans were accumulated. Measurements were performed in air, in a vacuum, and in a vacuum after degassing and heating in situ for 30 min.

FT-Raman (Fourier transform Raman) spectra were recorded on a Nicolet Nexus FT-Raman spectrometer with a Ge detector and a 1064 nm Nd:YAG laser. Samples were collected in a 180° reflective sampling configuration. 4000 scans were averaged for each sample with a resolution of 8 cm^{-1}. The laser power was set between 0.8 and 1.2 W.

The nitrogen adsorption−desorption isotherms were studied with a Quantachrome Autosorb 1 MP instrument. Before measurement, the samples were degassed for 16 h at 200 °C. N_2-sorption isotherms were recorded at −196 °C.

3. Results

3.1. CW-EPR Characterization of Noncalcined SBA-VS. The CW-EPR experiments performed on the noncalcined vanadium silicalite nanoparticles deposited in the mesopores of SBA-15 materials are summarized in Figure 1. The EPR spectrum recorded at 10 K of the as-prepared sample (Figure 1a) is dominated by a broad absorption signal centered at approximately $g = 1.98$. This feature was also observed in the case of $VO(acac)_2$ complexes deposited in the SBA-15 system[39] and is generally ascribed to a high local concentration of VO^{2+} units, whereby the signal is dipolarly broadened.[40,41] Superimposed to this signal a poorly resolved group of lines can be observed, which is due to the hyperfine interaction between the unpaired electron spin of V^{4+} ($3d^1$) and the ^{51}V nuclear spin ($I = {}^7/_2$, 99.8% natural abundance). This signal stems from more isolated VO^{2+} sites. Dehydration of the sample at room temperature under dynamic vacuum ($\cong 10^{-5}$ mbar) leads to the spectrum reported in Figure 1b. Inspection of the figure reveals that upon dehydration the broad signal due to the dipolar interacting VO^{2+} species is reduced in intensity, while the contribution of the isolated vanadyl sites becomes more evident.

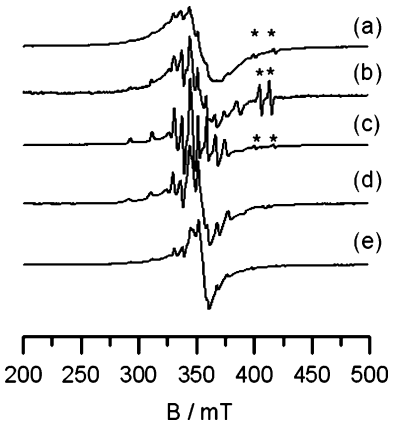

Figure 1. CW-EPR spectra of an SBA-VS sample recorded following different treatments. (a) Sample as-prepared; (b) sample dehydrated under a dynamic vacuum at room temperature; (c) sample dehydrated under a dynamic vacuum at 373 K; (d) sample rehydrated; (e) after aging 2 weeks in open air. All the spectra were recorded at 10 K. The asterisks in the figure indicate spurious cavity signals.

Table 1. Spin-Hamiltonian Parameters of VO^{2+} Centers in SBA-VS upon Different Treatments[a]

sample	$g_\parallel$	$g_\perp$	$\lvert A_\parallel \rvert$	$\lvert A_\perp \rvert$
as-received	1.9383	1.9778	537.2	194.1
dehydrated	1.9303	1.9763	529.5	186.7
rehydrated	1.9323	1.9767	543.6	203.4

[a] The parameters are obtained from computer simulation of the ESE spectra reported in Figure 3. The hyperfine coupling constants are expressed in MHz.

Further dehydration of the sample at 373 K under a dynamic vacuum (Figure 1c) leads to the vanishing of the broad absorption centered at $g = 1.98$, and a well resolved spectrum, characterized by an 8-fold hyperfine splitting of all anisotropic components, is obtained. This signal is characteristic of isolated VO^{2+} ions in square-pyramidal coordination. The g and A matrix values deduced from combined computer simulations of the CW-EPR and ESE-detected EPR spectra are listed in Table 1 (SBA-VS dehydrated) (see also section 3.2).

At this stage, the sample was rehydrated by keeping it overnight under a moist atmosphere. The broad line centered at $g = 1.98$ reappears (Figure 1d), but the well resolved component due to the isolated VO^{2+} centers reveals only small differences with respect to the one observed for the dehydrated sample. The most noticeable difference for this contribution concerns its temperature dependence. While only little change in the spectrum of the dehydrated sample is observed upon cooling (Figure 2a,b), the spectrum of the rehydrated sample, recorded at room temperature (Figure 2c), shows the clear

(36) Adamski, A.; Spalek, T.; Sojka, Z. *Res. Chem. Indermed.* **2003,** *29*, 793.
(37) Höfer, P.; Grupp, A.; Nebenfür, H.; Mehring, M. *Chem. Phys. Lett*. **1986**, *132*, 279.
(38) Madi, Z. L.; Van Doorslaer, S.; Schweiger, A. *J. Magn. Reson.* **2002**, *154*, 187.
(39) Van Doorslaer, S.; Segura, Y.; Cool, P. *J. Phys. Chem. B* **2004**, *108*, 19404.
(40) Luan, Z.; Kevan, L. *J. Phys. Chem.* **1997**, *101*, 2020.
(41) Baltes, M.; Cassiers, K.; Van Der Voort, P.; Weckhuysen, B. M.; Schoonheydt, R. A.; Vansant, E. F. *J. Catal.* **2001**, *197*, 160.

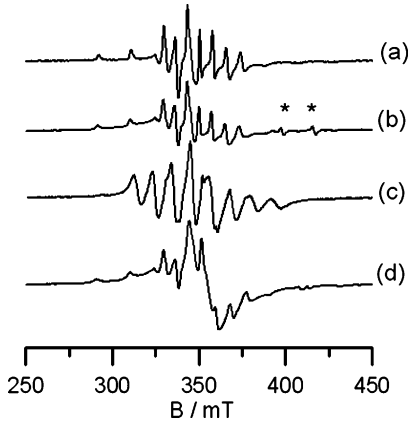

Figure 2. CW-EPR spectrum of an SBA-VS sample dehydrated under a dynamic vacuum at 373 K (a) recorded at 298 K, (b) recorded at 10 K. CW-EPR spectrum of the same sample rehydrated (c) recorded at 298 K, (d) recorded at 10 K. The asterisks in the figure indicate spurious cavity signals.

features of rotational averaging (the g matrix anisotropy is concealed and a single set of eight hyperfine lines is observed). This indicates a high mobility of the vanadyl units, which is suppressed upon cooling the sample to 10 K (Figure 2d).

The spin Hamiltonian parameters of the rehydrated sample are different from those of the dehydrated one (Table 1). In particular a small but clear increase in the ^{51}V hyperfine coupling constant is observed following the hydration process. The spin Hamiltonian parameters of the spectrum are very similar to those reported for hydrated exchanged VO^{2+} zeolites[42] and hydrated $VO(acac)_2$ deposited in SBA-15[39] and for the $VO(H_2O)_5^{2+}$ molecular ion ($g_\perp = 1.978$, $g_{||} = 1.933$, $A_\perp = 210.4$ MHz, $A_{||} = 547.4$ MHz).[43] This is thus a strong indication that upon hydration of the sample the VO^{2+} units become solvated by water molecules and are loosely bound to the SBA-15 or silicalite-1 substrate.

Aging of the sample for 2 weeks leads to the spectrum shown in Figure 1e, which is again dominated by the broad absorption likely to be due to clustered VO^{2+} groups thus confirming the mobility of the solvated species.

3.2 Pulse-EPR Experiments of Noncalcined SBA-VS. To investigate more deeply the effects caused by dehydration and rehydration of the sample and in the effort of better characterizing the local coordination environment of the VO^{2+} ions, pulsed EPR measurements were carried out.

Figure 3 shows the ESE-detected EPR spectra for the same sequence of experiments described in Figure 1 together with the computer simulation (dotted lines) of the most relevant spectra. As expected, the first derivative of the ESE-detected spectra closely resembles the corresponding CW-EPR spectra, except for the broad component at $g = 1.98$, which is not observed in the ESE-detected EPR spectra. The inability to detect this feature at the τ value used in recording the ESE-detected EPR spectra indicates that the phase memory time (T_m) for this species is much shorter than that of the resolved species. This confirms the earlier attribution of the $g = 1.98$ to dipolar interacting VO^{2+} species. In line with this finding, the intensity

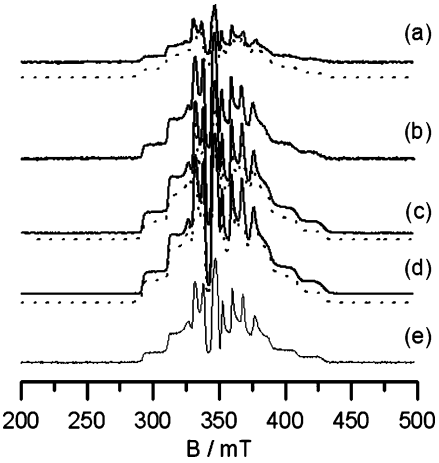

Figure 3. ESE-detected EPR spectra of the SBA-VS sample under different conditions. Labeling is the same as that in Figure 1. The dotted lines are the computer simulated spectra obtained using the spin-Hamiltonian parameters reported in Table 1. The experimental conditions were $t_{\pi/2} =$ 16 ns, $t_\pi = 32$ ns, $\tau = 200$ ns, $T = 10$ K.

of the Hahn echo signal increases with dehydration of the sample (Figure 3a−c) and parallels the decrease of the broad absorption feature detected in the CW-EPR spectra (Figure 1a−c).

The spin-Hamiltonian parameters obtained from computer simulations of the ESE-detected EPR spectra of the as-received, dehydrated, and rehydrated SBA-VS samples (Figure 3, dotted lines) are listed in Table 1. The simulation brings into evidence a clear difference in the spin-Hamiltonian parameters of the three forms, which suggests a modification in the first coordination sphere of the paramagnetic species.[43] This aspect is investigated in detail by means of HYSCORE experiments.

HYSCORE is a two-dimensional experiment where correlation of nuclear frequencies in one electron spin (m_S) manifold to nuclear frequencies in the other manifold is created by means of a mixing π pulse. The HYSCORE spectrum of the as-received sample SBA-VS recorded at observer position $B_0 = 346.5$ mT is reported in Figure 4a. This magnetic field setting corresponds to the so-called "powderlike position" in that almost all orientations are excited and the spectrum reflects a powderlike situation. The spectrum is dominated by a pronounced ridge in the (+,+) quadrant, centered at about 15 MHz (the ^{1}H Larmor frequency) with a width of about 8.2 MHz. Computer simulation of the spectrum (Figure 4b) shows that the broad proton ridge can be reproduced assuming the interaction of the unpaired electron with a single type of proton nuclei. In the simulation the contribution of remote protons was neglected, and attention was paid to reproduce the main features of the elongated ridge. The hyperfine coupling constants deduced from the simulation are reported in Table 2. Considerations based on quantum chemical calculations[44] and single-crystal ENDOR[45] data for $[VO(H_2O)_5]^{2+}$ indicate that the parallel principal proton hyperfine value is large and positive. Following these guidelines the isotropic and dipolar components of the A^H matrix can be obtained corresponding to $a_{iso} = 3.6$ MHz and $T = 4.6$ MHz. These values may be compared to experimental powder[46] and single-crystal ENDOR[45] data for the $[VO(H_2O)_5]^{2+}$ ion. Large positive a_{iso}, ranging from 7 to 8.5 MHz, and T values in the

(42) Woodworth, J.; Bowman, M. K.; Larsen, S. C. *J. Phys. Chem. B* **2004**, *108*, 16128.
(43) Chasteen, N. D. Vanadyl(IV) EPR Spin Probes: Inorganic and Biochemical Aspects. In *Biological Magnetic Resonance*; Berliner, L. J., Reuben, J., Eds.; Plenum: New York, 1981; Vol. 3, p 53.
(44) Larsen, S. C. *J. Phys. Chem. A* **2001**, *105*, 8333.
(45) Atherton, N. M.; Shackleton, J. F. *Mol. Phys.* **1980**, *39*, 1471.
(46) Mustafi, D.; Makinen, M. W. *Inorg. Chem.* **1988**, *27*, 3360.

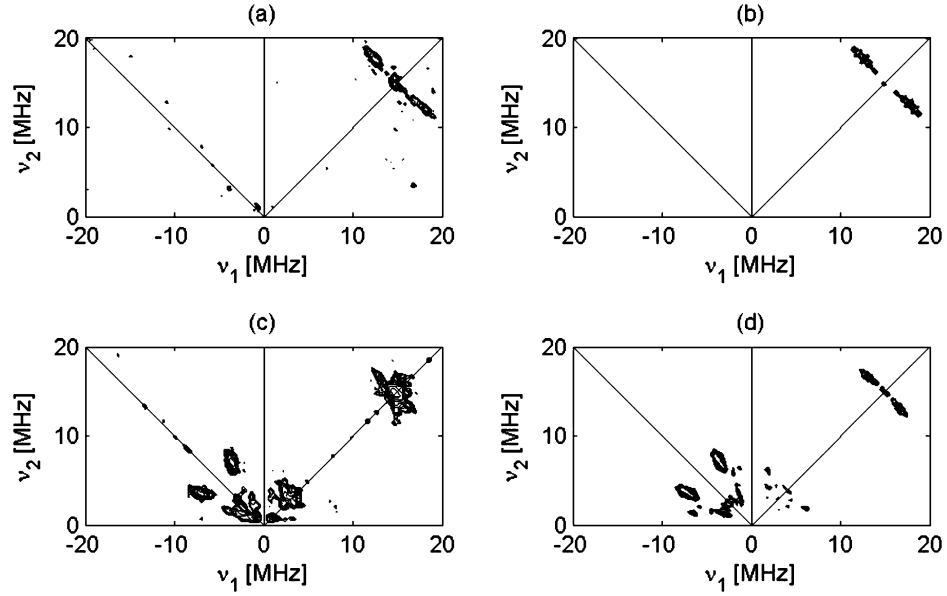

Figure 4. (a) HYSCORE spectrum of the as-prepared SBA-VS sample; (b) computer simulation of (a); (c) HYSCORE spectrum of SBA-VS dehydrated under a dynamic vacuum at 373 K; (d) computer simulation of (c). All spectra were taken at the same observer position (346.5 mT) with $\tau = 176$ ns.

Table 2. ^{1}H and ^{14}N Hyperfine and ^{14}N Nuclear Quadrupole Values of As-Received SBA-VS and of SBA-VS after Dehydration at 100 °C under a Dynamic Vacuum[a]

sample	$^{H}A_z$ [MHz]	$^{H}A_x$ [MHz]	$^{H}A_y$ [MHz]	$^{N}A_z$ [MHz]	$^{N}A_x$ [MHz]	$^{N}A_y$ [MHz]	β [deg]	K [MHz]	η	ref
SBA-VS as-received	±12.8	∓0.98	∓0.98							this work
SBA-VS dehydrated	±6.0	∓4.5	∓4.5	±5.5	±3.3	±3.9	30	2.8	0.6	this work
VO(edda)				±5.10	±5.10	±4.75		3.1	0.48	48
$VO(gly)_2$				±5.4	±5.20	±4.70		2.7	0.48	48
NH_3 adsorbed on silica-supported VO^{2+}				±4.86	±4.56	±4.56		0.72	0	49

[a] The parameters are obtained from simulation of the HYSCORE spectra reported in Figure 4b and 4d. Literature results for different complexes containing amine ligands on vanadyls are also reported for the sake of comparison.

range 4.7−5 MHz were found for the protons of water molecules laying in the VO^{2+} equatorial plane, while $a_{iso} \approx 0$ MHz and T values of about 4 to 5 MHz are characteristic of the protons of water molecules that coordinate perpendicularly to the vanadyl. Similar values were recently found in a HYSCORE study of hydrated vanadium exchanged ZSM-5 zeolites and assigned to either equatorially in plane or out of plane coordinated water molecules. Furthermore, both ENDOR experimental results[45] and quantum-chemical calculations[44,47] have shown that the proton isotropic hyperfine coupling constants for $[VO(H_2O)_5]^{2+}$ are very sensitive to the rotation of the equatorial water molecules around the V−O bond. The experimental results for the as-prepared SBA-VS system agree rather well with those found for equatorially coordinated OH groups suggesting that the VO^{2+} of the VS-1 nanoparticles inside the SBA-15 mesopores are partially hydrated.

The small variations observed in both CW and ESE-detected EPR spectra upon dehydration of the sample result in major changes of the HYSCORE spectrum. X-band HYSCORE spectra were recorded at different observer positions for the system under study. Figure 4c shows the spectrum of the dehydrated sample at the same observer position of the spectrum reported in Figure 4a (346.5 mT). Inspection of the figure reveals that some relevant changes occur in the spectrum as a consequence of the dehydration treatment. As it may be expected due to the loss of the coordinating water, the proton ridge becomes smaller with a maximum extension of about 5 MHz. This corresponds to the maximum hyperfine interaction of the unpaired electron with the surrounding protons, which is thus strongly reduced with respect to the as-received (partially hydrated) sample. The A^H matrix values deduced from computer simulation (Figure 4d, Table 2) allow us to determine $a_{iso} = -1$ MHz and $T = 3.5$ MHz, based on the same considerations adopted previously. Considering a purely dipolar interaction, the V−H distance can be estimated to be 0.28 nm from the following equation:

$$T = \frac{\mu_0}{4\pi} g_e g_n \beta_e \beta_n \frac{1}{r^3} \qquad (1)$$

with r being the distance between the unpaired electron localized in the V d orbitals and the ^{1}H nucleus.

The most relevant alteration occurs however in the (−,+) quadrant where the features of a new, complex signal show up. The new spectrum is dominated by a pair of cross-peaks centered at about (−3.5, 6.9) and (−6.9, 3.5) MHz. These peaks are assigned to the double-quantum transitions (**dq**) arising from the hyperfine interaction of the unpaired electron with a nitrogen nucleus ($I = 1$). The assignment is corroborated by computer simulation of the spectrum (Figure 4d) which allows us to determine the $\boldsymbol{A}^N$ and $\boldsymbol{Q}^N$ tensors. Simulations were performed for two different spectra taken at the powderlike (346.5 mT)

(47) Saladino, A. C.; Larsen, S. C. *Catal. Today* **2005**, *105*, 122.

and at the $g_{||}$, $m_I = -^7/_2$ observer position (292.6 mT). The best fit of the experimental spectra was obtained imposing the Euler angle $\beta = 30°$, where β is the angle between A_z and the normal plane, for a rotation about the *y* axis. The complete set of spin-Hamiltonian parameters is listed in Table 2. The simulation was carried out assuming ideal pulses, which explains the differences in relative peak intensities between the experimental and the simulated spectrum.

The HYSCORE spectrum of a $S = {}^1/_2$, $I = 1$ disordered system is typically dominated by the cross-peaks between the **dq** frequencies

$$\nu_{dq}^{\alpha,\beta} = 2\sqrt{\left(\frac{a}{2} \pm \nu_I\right)^2 + K^2(3+\eta^2)} \qquad (2)$$

where a is the hyperfine coupling at a given observer position, while $K = e^2qQ/4h$ is the quadrupolar coupling constant and η is the so-called asymmetry parameter. K and η are related to the principal values Q_x, Q_y, and Q_z of the traceless $\boldsymbol{Q}$ tensor by the following relations: $Q_x = -K(1-\eta)$, $Q_y = -K(1+\eta)$ and $Q_z = 2K$.

Comparison with literature data for different vanadyl complexes containing amine ligands[42−49] (Table 2), strongly suggests that the signal in Figure 4c is due to equatorially bound nitrogens. The lack of combination peaks in the spectrum may be taken as an indication that one single nitrogen is bound to the VO^{2+} unit. This also agrees with the small perturbation observed for both the CW and ESE-detected EPR spectra (Figures 1 and 3). More pronounced changes in both $\boldsymbol{g}$ and $\boldsymbol{A}^V$ tensors would in fact be expected in the case of replacement of all the equatorial ligands.[43]

No clear evidence can be obtained from the spectrum concerning the interaction with ^{29}Si ($\nu_I = 2.963$ MHz) nuclei of the matrix and/or other ^{51}V ($\nu_I = 3.917$ MHz) nuclei as these signals overlap with the nitrogen features. However, in situ DRIFT (Diffuse Reflectance Infrared analysis) (not shown) features significant bands at 963 cm^{-1} and at 967 cm^{-1} for the dehydrated sample and the as-prepared sample, respectively. These bands are attributed to the stretching vibration mode of a SiO_4 unit bound to a vanadyl ion.[50,51]

Rehydration of the SBA-VS sample causes major changes in the HYSCORE spectrum (Figure 5a). In particular the spectral features arising from the interaction with the ^{14}N nucleus have almost completely disappeared, while a prominent proton ridge with a maximum extension of about 11.3 MHz shows up in the (+,+) quadrant centered at ν_H. This result indicates that admission of water onto the sample displaces the nitrogen ligand and is in agreement with the weak binding of $-NH_2$ groups to VO^{2+} reported in the literature.[43]

For the sake of comparison we recorded the HYSCORE spectrum of the ($[VO(H_2O)_5]^{2+}$) ion in frozen solution obtained from dilution of $VOSO_4$ in a water-based solvent mixture containing 20% of glycerol (Figure 5b). Glycerol was added to ensure good glass formation. Comparison of the two spectra reveals that indeed the spectrum of the rehydrated SBA-VS sample can be interpreted in terms of pentacquo VO^{2+} complexes hosted within the SBA framework containing the vanadium silicalite-1 nanoparticles. This is in agreement with the CW-EPR spectrum reported in Figure 2c, which indicates a high degree of mobility at room temperature as is expected in the case of water-solvated VO^{2+} species. It also matches the spin Hamiltonian parameters obtained from simulation of the ESE-detected spectrum.

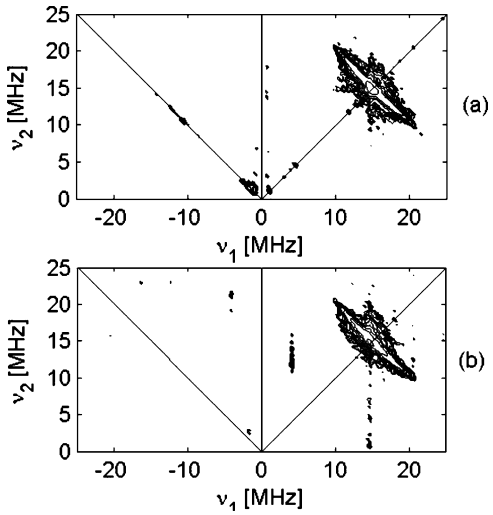

Figure 5. (a) HYSCORE spectrum of the SBA-VS sample rehydrated. (b) HYSCORE spectrum of a $VOSO_4$ water solution with 20% glycerol. Both spectra were taken at observer position $B_0 = 346.5$ mT, and two τ values (96 ns and 176 ns) are summed together.

3.3. Pulsed-EPR Experiments on Noncalcined Full-Grown Vanadium Silicalite 1. Experiments analogous to those described above have been carried out on the full-grown vanadium silicalite-1 zeolite in order to better compare the structural properties of the vanadium silicalite-1 nanoparticles within the mesoporous structure of SBA-15 with the full-grown VS-1 zeolite. Some important differences were found, when the same dehydration and subsequent rehydration treatments were carried out on full-grown vanadium silicalite-1 zeolite crystals. Dehydration and subsequent rehydration of the zeolite are found to induce only minor changes in both CW and pulsed EPR spectra.

The HYSCORE spectra relative to the entire cycle of dehydration and rehydration are shown in Figure 6. At variance with the case of the zeolites nanoparticles deposited in the SBA-15 material, the HYSCORE spectrum of the dehydrated, full-grown VS-1 zeolite (Figure 6b) does not show any trace of interaction with nitrogen nuclei. Conversely the spectrum shows a ridge centered at (ν_{Si}, ν_{Si}) resulting from the hyperfine interaction of the VO^{2+} ions with a $^{29}Si^{4+}$ ion ($I = {}^1/_2$, natural abundance 4.68%) of the zeolite framework. The edge of the ^{29}Si ridge is at about (4.04, 1.78) MHz indicating a maximum hyperfine interaction of 2.26 MHz. Simulation of the signal (see Supporting Information) allows us to refine these data and obtain the full tensor: [∓ 0.23 ∓ 0.23 ± 2.41] MHz. From this tensor $T = 0.88$ MHz is obtained which, applying eq 1, corresponds to a distance of 0.28 nm between the VO^{2+} ion and the ^{29}Si nucleus of the zeolite framework. Considering the Si−O bond distance of 0.16 nm and assuming a V−O bond length of 0.17 nm,[50,52] the V−O−Si angle can be estimated to be 104°. This value seems to be in agreement with a model where V atoms

(48) Fukui, K.; Ohya-Nishiguchi, H.; Kamada, H. *Inorg. Chem.* **1997**, *36*, 5518.
(49) Larsen, S. C.; Singel, D. J. *J. Phys. Chem.* **1992**, *96*, 9007.
(50) Higashimoto, S.; Matsuoka, M.; Zhang, S. G.; Yamashita, H.; Kitao, O.; Hidaka, H.; Anpo, M. *Microporous Mesoporous Mater.* **2001**, *48*, 329.
(51) Kornatowski, J.; Wichterlova, B.; Jirkovsky, J.; Löffer, E.; Pilz, W. *J. Chem. Soc., Faraday Trans.* **1996**, *92*, 6, 1067.
(52) Centi, G.; Perathoner, S.; Trifiro, F.; Aboukais, A.; Aissi, C. F.; Guelton, M. *J. Phys. Chem.* **1992**, *96*, 2621.

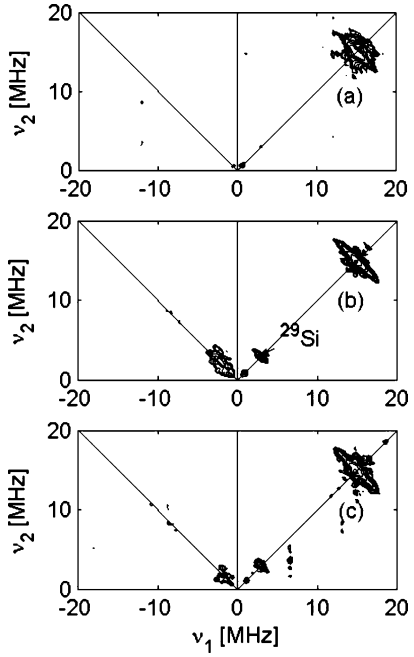

Figure 6. HYSCORE spectra of full-grown Vanadium silicalite (a) as-prepared sample; (b) sample dehydrated at 373 K; (c) sample rehydrated. All spectra were taken at observer position $B_0 = 346.5$ mT, and two τ values (96 ns and 176 ns) are summed together.

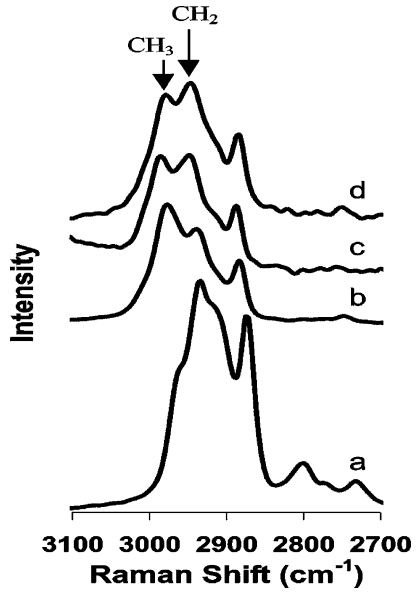

Figure 7. Raman spectra of (a) tripropylamine, (b) the full-grown VS-1 zeolite before calcination, (c) TPAOH 20% solution, (d) SBA-VS-15 before calcinations.

are anchored to the zeolite framework in which they act as framework satellites.[52,53] Interestingly, only a very weak ^{29}Si signal was observed before dehydration (Figure 6a), which indicates that there is some initial H_2O or silanol binding to the vanadyl centers, which is removed by dehydration. Based on the width of the proton ridge, this binding must be axial and not equatorial to the vanadyl. Dehydration thus seems to facilitate even more the incorporation of the vanadyl in the silica structure. Furthermore, only minor changes in the HYSCORE spectrum of the full-grown VS-1 zeolite were observed upon rehydration of the sample (Figure 6c). Visual comparison of Figure 6c and 6b indicates that, differently from the case of the vanadium silicalite nanoparticles hosted in the SBA-15 mesopores, the VO^{2+} ions have a low affinity toward hydration. Moreover, the interaction with the $^{29}Si^{4+}$ ions of the zeolite framework remains unchanged upon rehydration, revealing a relatively strong interaction of the VO^{2+} with the zeolite framework.

3.4. Raman Experiments. HYSCORE measurements suggest the covalent bonding of one single nitrogen to the vanadyl complex after dehydration of the SBA-VS-15 samples. Since nitrogen is only present in the template (tetrapropylammoniumhydroxide, TPAOH) of the VS-1 nanoparticles, these results suggest the removal of one of the four propyl ligands from the zeolite template. Raman spectra of the full-grown zeolite (Figure 7b) and the deposited VS-1 nanoparticles in SBA-15 (Figure 7d) were recorded in order to confirm this hypothesis. For comparison the spectra of TPAOH (Figure 7c, the free template in a 20% aqueous solution) and tripropylamine (Figure 7a, the template with the loss of one ligand, across organics) were measured. The CH stretching bands of free TPAOH (Figure 7c) at 2985, 2949, and 2887 cm^{-1} have shifted to lower Raman frequencies in the full-grown VS-1 zeolite (2977, 2939, and 2883 cm^{-1}) (Figure 7b). This is in agreement with previous findings and can be explained by the decreasing force constant of the CH bonds in the *n*-propyl ligands with increasing crystal size of the zeolite, due to the interaction of the *n*-propyl ligands with the zeolite framework.[54] Moreover, there is a difference in the relative intensity of the CH_2 to the CH_3 stretching vibration when comparing the free TPAOH and the TPAOH bound in the zeolites framework. As was reported in the literature, the intensity of the CH_3 vibration (2977 cm^{-1}) increases relative to the intensity of the CH_2 stretching vibration (2939 cm^{-1}) with the increasing growth of the zeolite.[54] The CH_2/CH_3 intensity ratio of the full-grown zeolite was calculated to be 0.79 in comparison with the free TPAOH template where the intensity ratio of CH_2/CH_3 is 1.0. As can be seen in Figure 7d the CH_3 and CH_2 stretching vibrations of SBA-VS-15 have shifted to lower Raman shifts, 2978 and 2947 cm^{-1}, respectively, similar to the full-grown zeolite. However, in contrast to the Raman shift of CH_3 the shift of the CH_2 stretching is less pronounced than in the case of the full-grown zeolite. In addition, the intensity ratio of CH_2/CH_3 stretching vibrations has increased to 1.1 instead of the expected decrease similar to the full-grown VS-1 zeolite. These results could be explained by the loss of one ligand in some of the template TPAOH molecules present in the VS-1 nanoparticles. Supposing one of the ligands of the TPAOH template is lost, the Raman spectrum of tripropylamine is expected (Figure 7a). Tripropylamine shows only one asymmetric band at 2934 cm^{-1} with shoulders at 2957 and 2919 cm^{-1} and a band at 2873 cm^{-1}. When the spectrum of the full-grown zeolite is subtracted from the spectrum of the SBA-VS-15 sample, a spectrum with similar peak positions as the tripropylamine was obtained. These results suggest the presence of a mixture of both tripropylamine and the TPAOH ligands bound to the VS-1 nanoparticles framework, explaining the unexpected increase in the CH_2/CH_3 intensity ratio present

(53) Sen, T.; Ramaswamy, A. V.; Rajamohanan, P. R.; Sivasanker, S. J. *J. Phys. Chem.* **1996**, *100*, 3809.

(54) Baranska, H.; Czerwinska, B.; Labudzinska, A. *J. Mol. Struct.* **1986**, *143*, 485.

Chart 1. Depiction of the Local VO^{2+} Environment for Noncalcined VS-1 Nanoparticles Deposited on the Walls of SBA-15 after Dehydration

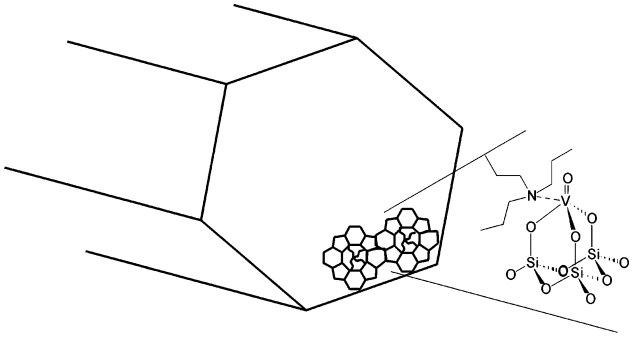

in the SBA-VS-15 spectrum since no band at 2980 cm^{-1} is present in the tripropylamine spectrum.

4. Discussion

The salient points of the results presented in the previous section can be summarized as follows:

(1) Vanadium silicalite-1 nanoparticles deposited inside the SBA-15 material are highly hydrophilic in contrast to the full-grown vanadium silicalite-1 zeolite. The proton HYSCORE spectra of the as-prepared SBA-VS-15 system indicate that the VO^{2+} ions in the zeolite nanoparticles are interacting with at least one nearby OH group. The spin-Hamiltonian parameters deduced for the interacting proton agree rather well with those found in different studies[42,46] for an equatorially bound OH indicating that the vanadyl is partially hydrated. Both CW-EPR spectra and complementary DRIFT studies indicate, however, that under these circumstances the VO group is bound to the zeolites framework. Adsorption of water to a previously dehydrated sample leads to fully hydrated species. The HYSCORE spectrum of these species is identical with that of $[VO(H_2O)_5]^{2+}$ ions, providing strong, compelling evidence that pentacquo vanadyl complexes are formed under these circumstances. These are highly mobile (Figure 2), and clustering is favored inside the mesoporous structure.

(2) Dehydration of the system leads to a change in the coordination environment of the VO^{2+} ions. The HYSCORE spectrum (Figure 4) shows that, upon dehydration, an equatorial interaction between VO^{2+} and a nitrogen ligand can be observed. Nitrogen is only present in the template molecules (TPAOH). This suggests that one of the propyl ligands is removed from the template by acidification of the VS-1 nanoparticle solution and replaced by vanadyl upon dehydration, which was confirmed by Raman. A schematic representation of the bonding of vanadyl to the zeolite nanoparticle after dehydration is shown in Chart 1.

(3) A totally different behavior is found for the full-grown VS-1 zeolite. Hydration and dehydration experiments are found to only moderately affect the coordination environment of the VO^{2+} group, and no coordinated nitrogens are observed.

These differences in hydrophilic behavior between the impregnated VS-1 nanoparticles and the full-grown VS-1 zeolite can be explained by the differences in size between the nanoparticles and the full-grown zeolite. Since the nanoparticles are small, the external surface where the uncondensed silanol groups are present is large versus the bulk volume.[35,55] Therefore the particles have a more hydrophilic nature compared to the hydrophobic full-grown VS-1 zeolites. Due to the fact that the small size will cause the vanadyl species to be more on the surface of the small nanoparticles and due to the higher hydrophilic nature of the nanoparticles, water has a better access to the vanadyl species, which have a high affinity for water. As was shown by CW-EPR and HYSCORE, a decreased stability of the VS-1 nanoparticles compared to the full-grown VS-1 zeolite toward leaching in polar media can therefore be expected. In addition, the high mobility of vanadyl species in the aqueous synthesis gel of the VS-1 nanoparticles also suggests that the vanadyl species are not fixed completely within the hydrophilic network in this stage of the zeolite synthesis where the nanoparticles are still hydrophilic and have not yet grown during hydrothermal treatment. The true incorporation of the vanadyl species in the zeolite structure would therefore be expected during hydrothermal growth of the nanoparticles in which the solvated vanadyl species will get trapped between aggregating nanoparticles. Although the structure is more hydrophilic, spin Hamiltonian parameters of the as-prepared samples show that the vanadyl species present in the impregnated VS-1 nanoparticles are similar to those of hydrated exchanged VO^{2+} zeolites.[42]

Raman measurements of the SBA-VS-15 samples showed the presence of both TPAOH and tripropylamine indicating the loss of a propyl ligand in some of the TPAOH templates present in the VS-1 nanoparticles. In addition, HYSCORE spectra of the dehydrated samples revealed a bonding of nitrogen to the vanadyl species. Raman and HYSCORE spectra of the full-grown zeolite showed no change in the TPAOH ligand and were similar to results reported in the literature. These results suggest that the stability of the TPAOH template is affected by the acidification of the nanoparticles solution before impregnation in the SBA-15 materials, since the full-grown zeolite was prepared by hydrothermal treatment of the basic nanoparticles solution. Moreover, only part of the TPAOH molecules has suffered the loss of a ligand. This suggests that only those TPAOH molecules with only three ligands in the zeolite framework and one propyl ligand on the external surface have lost a ligand by means of acid hydrolysis, since the other TPAOH molecules are protected by the zeolite framework. These results could explain the reason for the previously reported stop in the continuous growth of the nanoclusters into large crystals under strong acidic conditions and the reason why mesoporous materials can be made with these nanoclusters as building blocks without the zeolite crystals as byproducts.[56]

5. Conclusion

Vanadium silicalite-1 nanoparticles were impregnated within the mesoporous channels of SBA-15 rendering a material with special characteristics toward stability, accessibility, and diffusion. A CW- and pulse EPR spectroscopic study was done in order to conclude whether the deposited VS-1 nanoparticles had similar properties compared to the full-grown VS-1 zeolite. The results reported revealed that (1) the VS-1 nanoparticles are

(55) Ravishankar, R.; Kirschhock, C. E. A.; Knops-Gerrits, P.-P.; Feijen, E. J. P.; Grobet, P. J.; Vanoppen, P.; De Schrijver, F. C.; Miehe, G.; Fuess, H.; Schoeman, B. J.; Jacobs, P. A.; Martens, J. A. *J. Phys. Chem. B* **1999**, *103*, 4960.
(56) Han, Y.; Xiao, F.-S.; Wu, S.; Sun, Y.; Meng, X.; Li, D.; Lin, S.; Deng, F.; Ai, X. *J. Phys. Chem. B* **2001**, *105*, 7963.

hydrophilic in contrast to the hydrophobic full-grown VS-1 zeolite. Therefore, the vanadyl species in the deposited VS-1 nanoparticles experience more structural changes upon dehydration and rehydration. (2) HYSCORE and Raman spectra revealed the instability toward acidification of the TPAOH zeolite template in the nanoparticles. Results suggest the loss of a propyl ligand from the TPAOH molecules present on the outer surface of the VS-1 zeolite nanoparticles. Upon dehydration a weak bonding between the nitrogen of the TPAOH molecule and the vanadyl species becomes visible. Raman measurements show the presence of both TPAOH and tripropylamine after acidification and deposition. (3) The full-grown VS-1 zeolite shows clear differences with the deposited VS-1 nanoparticles with respect to its hydrophobic nature and its resistance toward hydration and acidification.

These results promise to be valuable in the evaluation of these materials as potential catalysts. Moreover, they provide a general explanation for the growing mechanisms and structural characteristics of several mesoporous materials reported in the literature, in which TPAOH-templated zeolite nanoparticles were used as building blocks for the synthesis of mesoporous networks in acidic environments.

Acknowledgment. Financial support of the European Commission is gratefully acknowledged, within the frame of the INSIDE-PORES NoE project (FP6-EU). V.M. acknowledges the FWO-Flanders (Fund for Scientific Research-Flanders) for financial support. S.V.D. and P.C. want to thank the FWO for funding through the G.0312.05 research project.

Supporting Information Available: Nitrogen adsorption−desorption isoterms for pure SBA-15 and deposited VS-1 nanoparticles (SBA-VS-15). Simulation of ^{29}Si HYSCORE spectrum of dehydrated VS-1 full grown zeolites. This material is available free of charge via the Internet at http://pubs.acs.org.

JA061630P